Remote Sensing Modeling of Land Surface Properties

Geo 827, MSU
Jiquan Chen
Dec. 8, 2015

- Why RS?
- Advantages:
- Disadvantages:
- Cases: GPP and ET from MODIS
- Other applications

Case studies

1) Connection data-models-RS products

2) MODIS ET

3) MODIS GPP

4) NEP in N Wisconsin

5) Carbon & Water on Mongolia Plateau

A few selected applications of RS in ecosystem studies

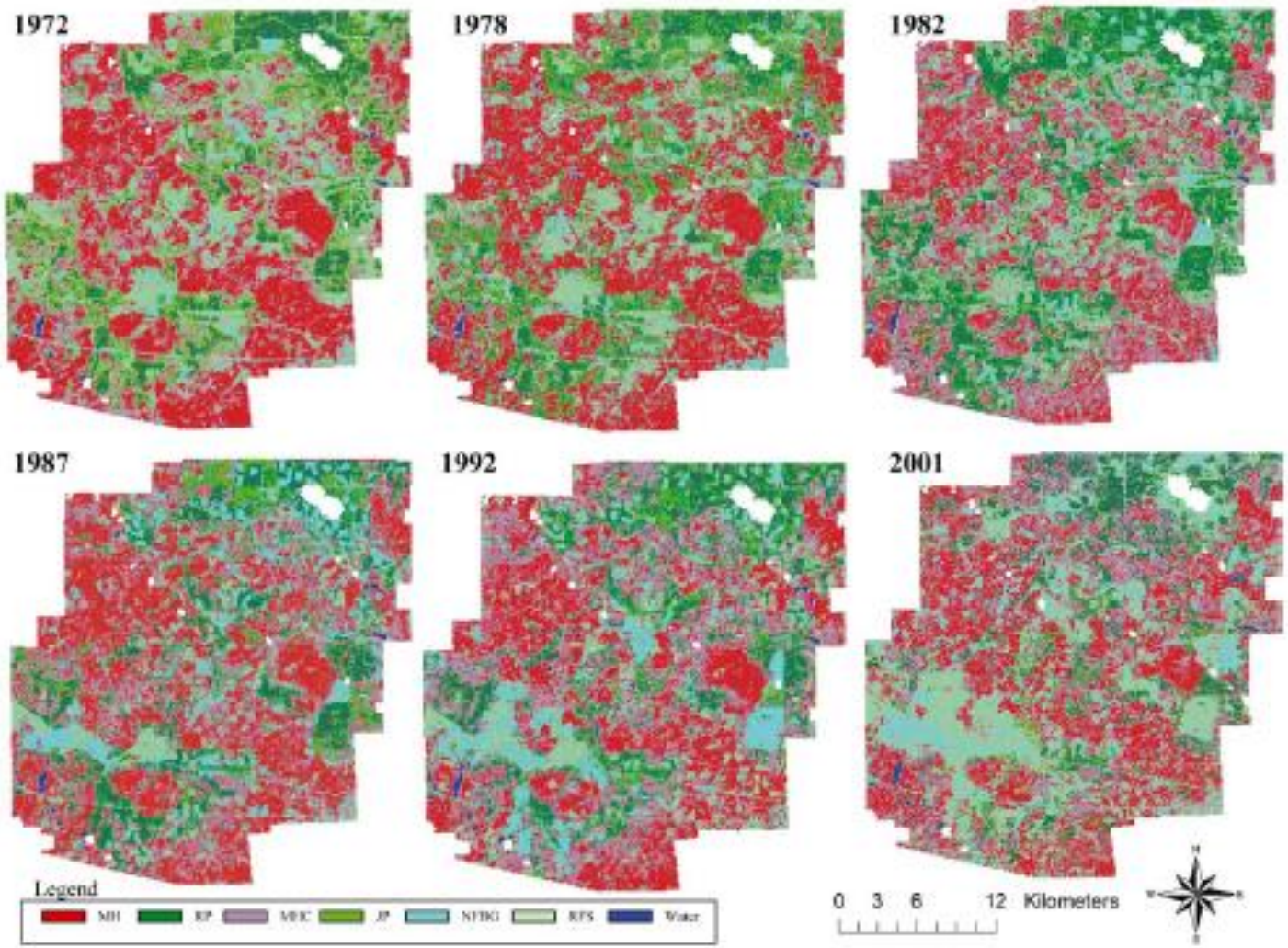

Figure 2. Six classified images (1972-2001) of the landscape. Cover types include mixed hardwood (MH), jack pine (JP), red pine (RP), mixed hardwood/conifer (MHC), regenerating forest or shrub (RFS), and non-forested bare ground (NFBG).

A few selected applications of RS in ecosystem studies

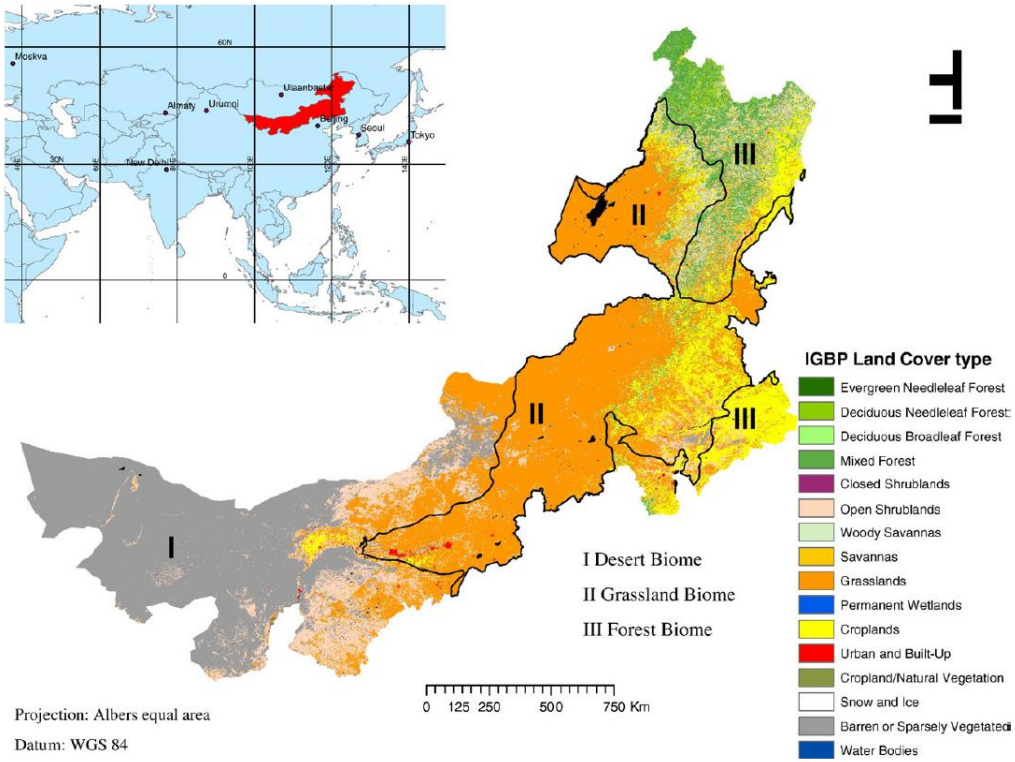

A few selected applications of RS in ecosystem studies

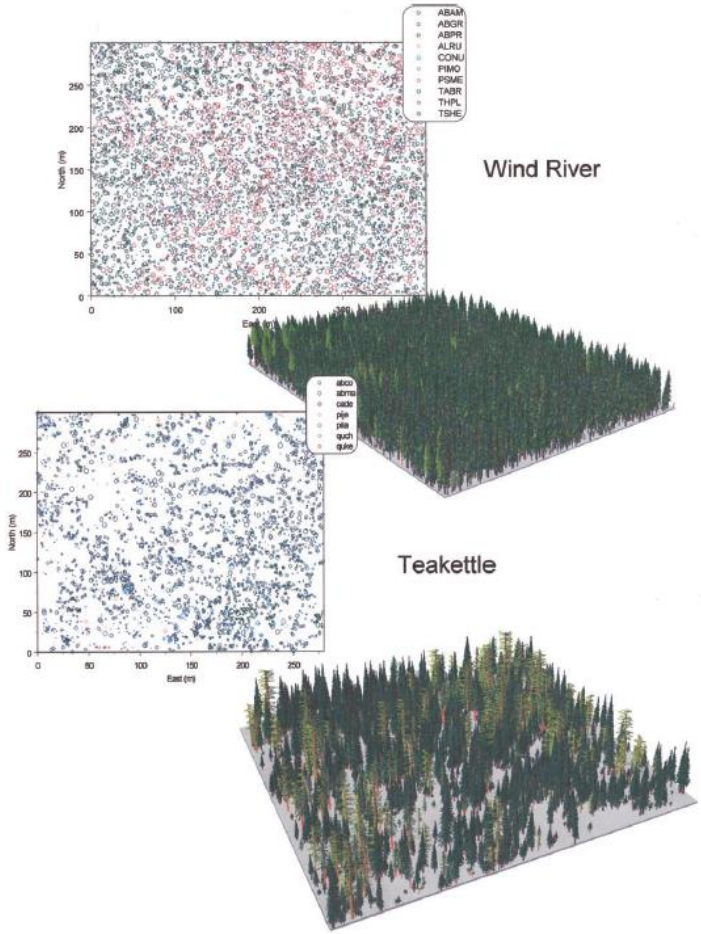

Figure 2. Map and stand visualization simulations (SVS) of all live stems ≥5 cm dbh at Wind River and Teakettle. Circles are proportional to diameter and color coded by species. To facilitate comparison, plots and diameter circle sizes have been scaled to the same dimension. Species codes at Wind River are *Abies amabilis* (ABAM), *A. grandis* (ABGR), *A. procera* (ABPR), *Alnus rubra* (ALRU), *Cornus nuttallii* (CONU), *Pinus monticola* (PIMO), PSME (*Pseudotsuga menziesii*), *Taxus brevifolia* (TABR), *Thuja plicata* (THPL), and *Tsuga heterophylla* (TSHE). Species codes at Teakettle are *Abies concolor* (ABCO), *A. magnifica* (ABMA), *Calocedrus decurrens* (CADE), *Pinus lambertiana* (PILA), *P. jeffreyi* (PIJE), *Quercus chrysolepis* (QUCH), and *Q. kelloggii* (QUKE). Crowns representations of each tree by species were developed from shapes in SVS and drawn over the location of each stem.

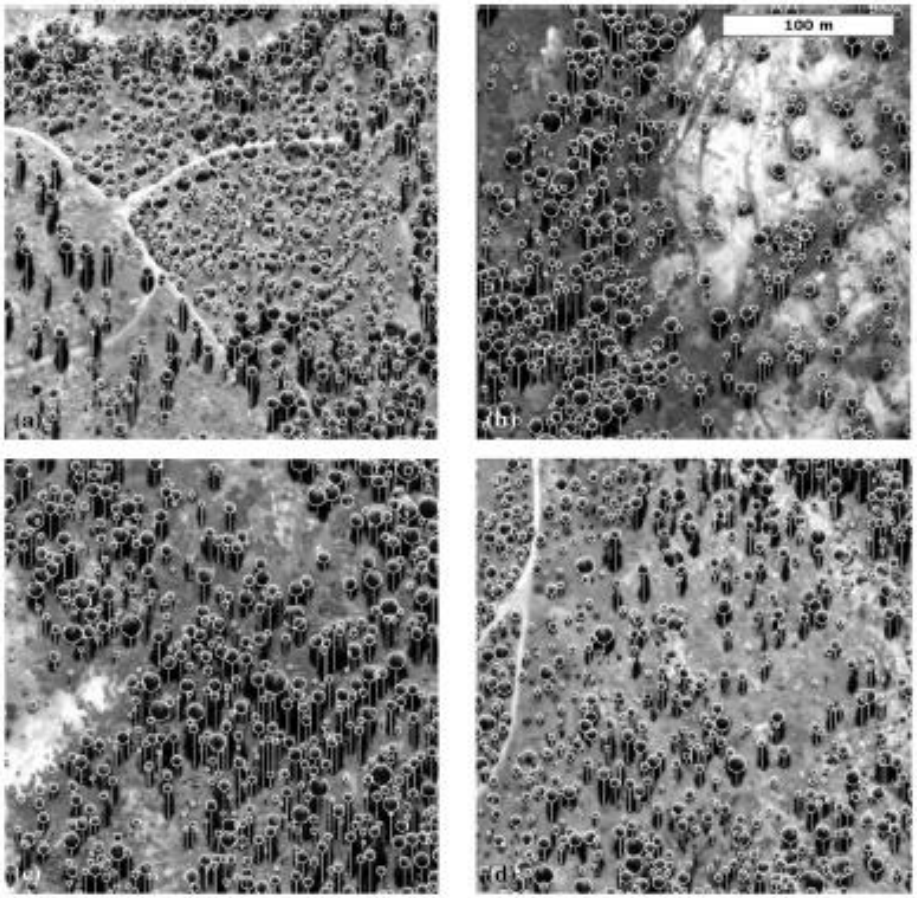

Fig. 3. Typical CANAPI crown (circle) and tree shadow (line) detections over QuickBird 0.6 m panchromatic images in the Teakettle Experimental Forest, Sierra National Forest, California. Shadows that are truncated by tree crowns or the edge of the image are not used in tree height calculation. The imagery was acquired June 25, 2003.

A few selected applications of RS in ecosystem studies

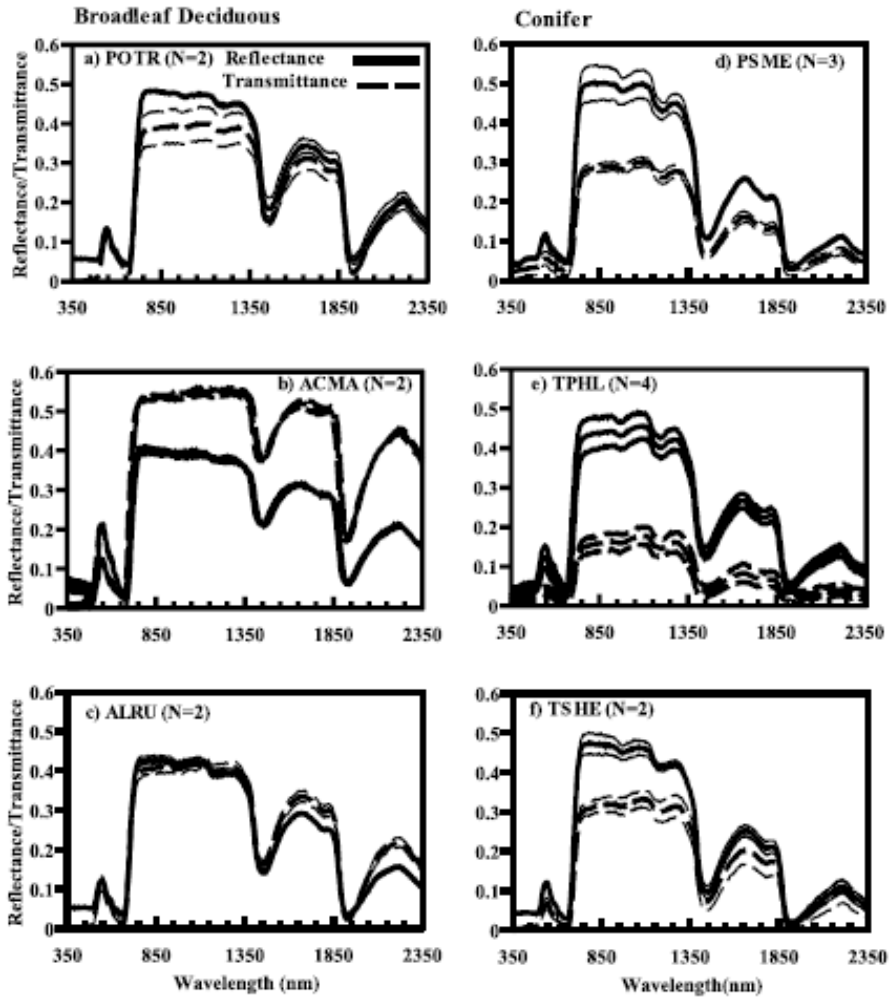

Figure 2. Leaf-level hemispherical reflectance and transmittance spectra of three broadleaf and three conifer dominants. Reflectance is plotted as a solid line; transmittance, as a dashed line. Plots show the mean ± SD. The number of spectra taken is shown in parentheses. Species names follow the codes in the text. POTR, *Populus trichocarpa*; ACMA, *Acer macrophyllum*; ALRU, *Alnus rubra*; PSME, *Pseudotsuga menziesii*; THPL, *Thuja plicata*; TSHE, *Tsuga heterophylla*.

A few selected applications of RS in ecosystem studies

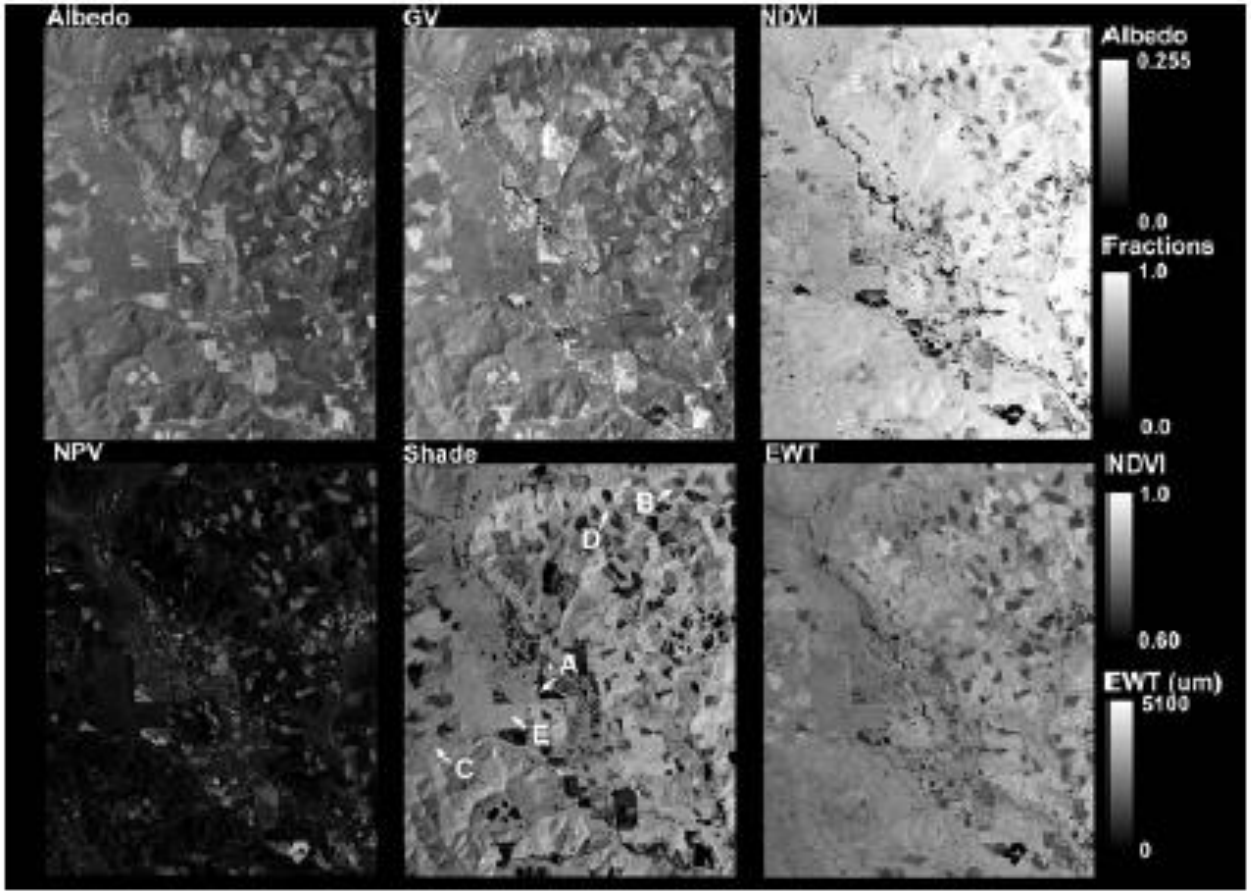

Figure 6. AVIRIS image data from a subset of the study site showing albedo, spectral fractions for non-photosynthetic vegetation (NPV), green vegetation (GV), and shade. The normalized difference vegetation index (NDVI), scaled between 0.6 and 1.0, and equivalent water thickness (EWT), scaled between 0 and 5,100, are shown to the right of spectral fractions. Five locations that represent a diversity of age classes are in the shade image. These stands are A) 8, B) 29, C) 70, D) 132, and E) 461 years old.

Beijing, China
Chen et al. unpublished

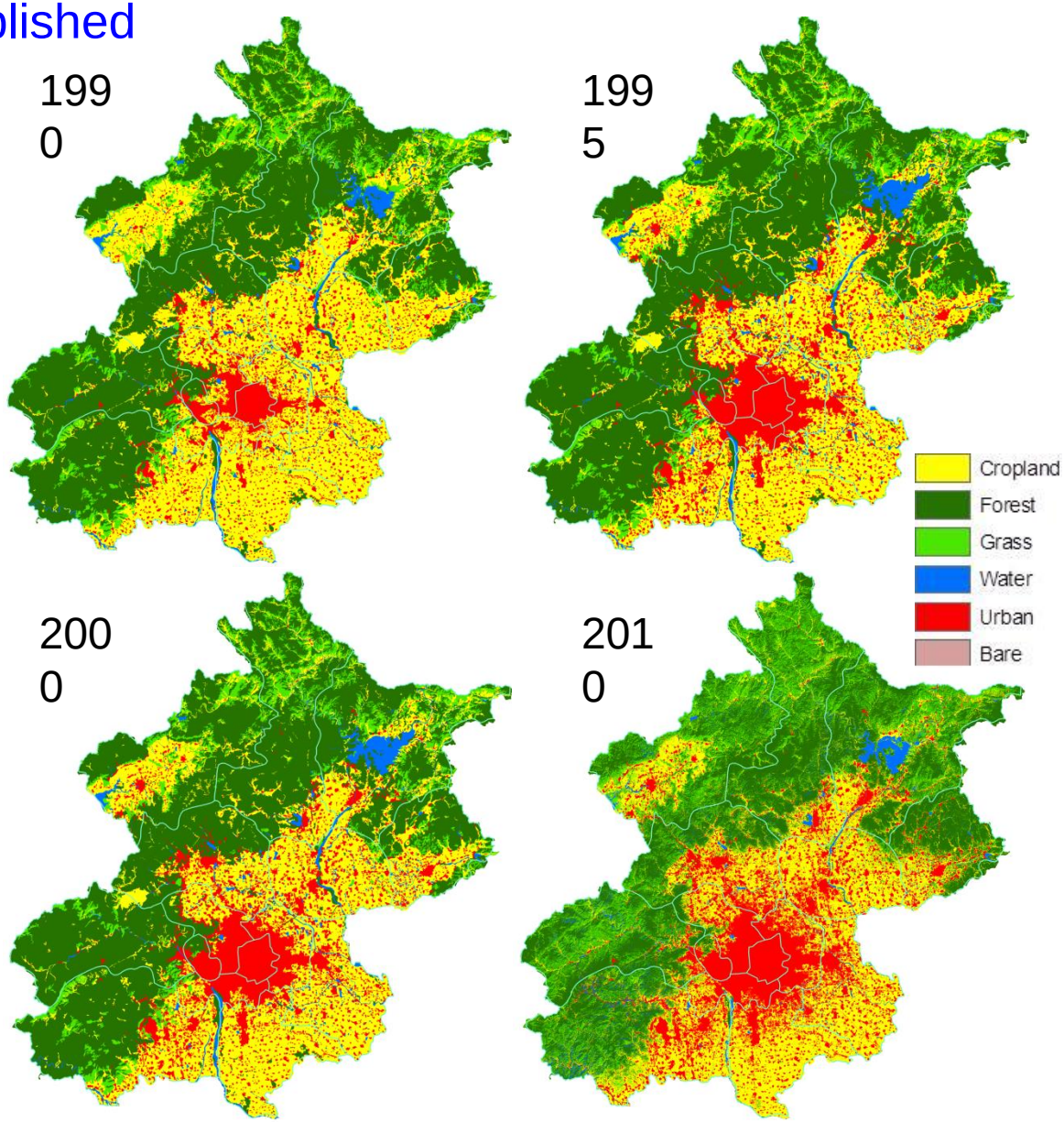

Landscape Ecol (2014) 29:1709–1723
DOI 10.1007/s10980-014-0061-8

RESEARCH ARTICLE

Vulnerability of a coupled natural and human system in a changing environment: dynamics of Lanzhou's urban landscape

Peilei Fan · Yaowen Xie · Jiaguo Qi · Jiquan Chen · Huiqing Huang

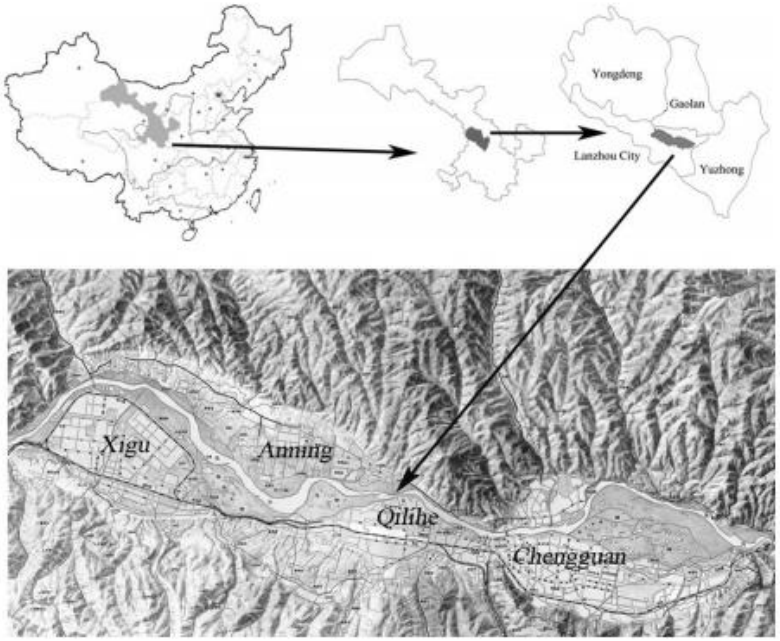

Fig. 1 Geographic locations of Gansu Province and its capital city—Lanzhou. The urban built-up areas were clustered in the northern and southern banks of the Yellow River

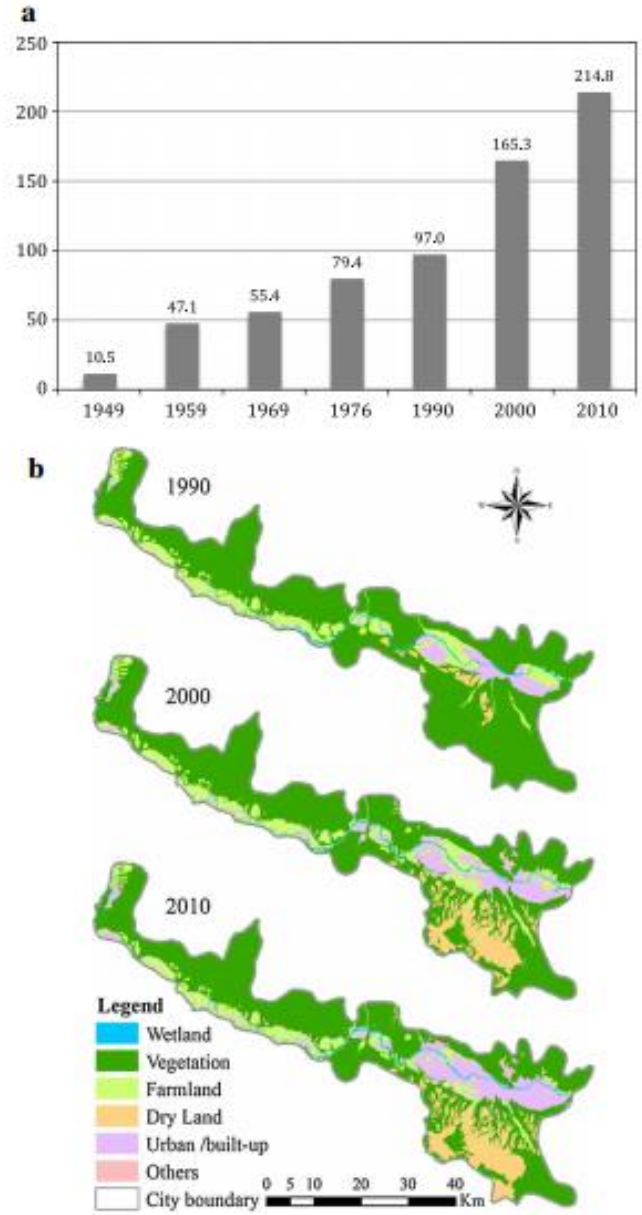

Fig. 5 Land use land cover change in Lanzhou: **a** Urban built-up area expansion 1949–2010 (in km^2), **b** land cover and land use change 1990–2010. Note that Fig. 5a was created based on data from Yang and Yang (2009) for 1949–1976

Environmental Research 144 (2016) 96–112

Contents lists available at ScienceDirect

Environmental Research

Urbanization and environ
transition on the Mongol

Peilei Fan [a,*], Jiquan Chen [b], Ranj

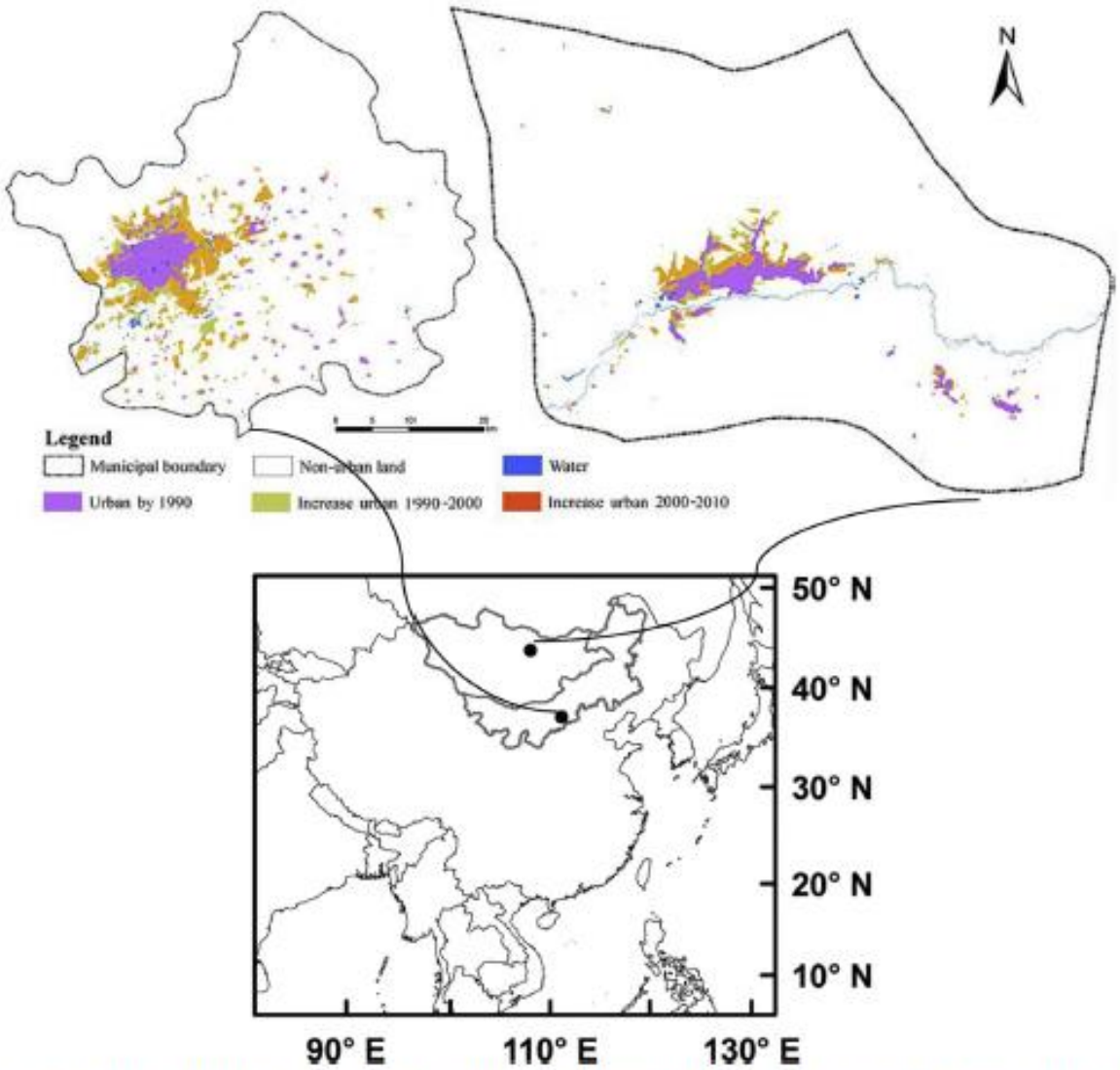

Fig. 2. Urban expansion of Hohhot and Ulaanbaatar, 1990–2010. The urban built-up areas clustered north of the Yellow River and the Tuul River for Hohhot and Ulaanbaatar, respectively. Hohhot (left) expanded much faster during 2000–2010 than that during 1990–2000. While development occurred mostly along the eastern urban fringe area from 1990 to 2000, urban built-up lands were added to the rest of the urban periphery area from 2000 to 2010. The settlement areas in the northern hilly areas accounted for most of Ulaanbaatar's urban expansion (right). The newly added urban built-up areas were concentrated in the original agricultural lands along the Tuul River and the mountainous areas in the north, within the traditional Ger areas.

Remote Sens. **2014**, *6*(3), 2239-2254; doi:10.3390/rs6032239

Open Access

Article

Estimating Canopy Characteristics of Inner Mongolia's Grasslands from Field Spectrometry

Feng Zhang [1], Ranjeet John [2], Guangsheng Zhou [1,3,*], Changliang Shao [1] and Jiquan Chen [2,4]

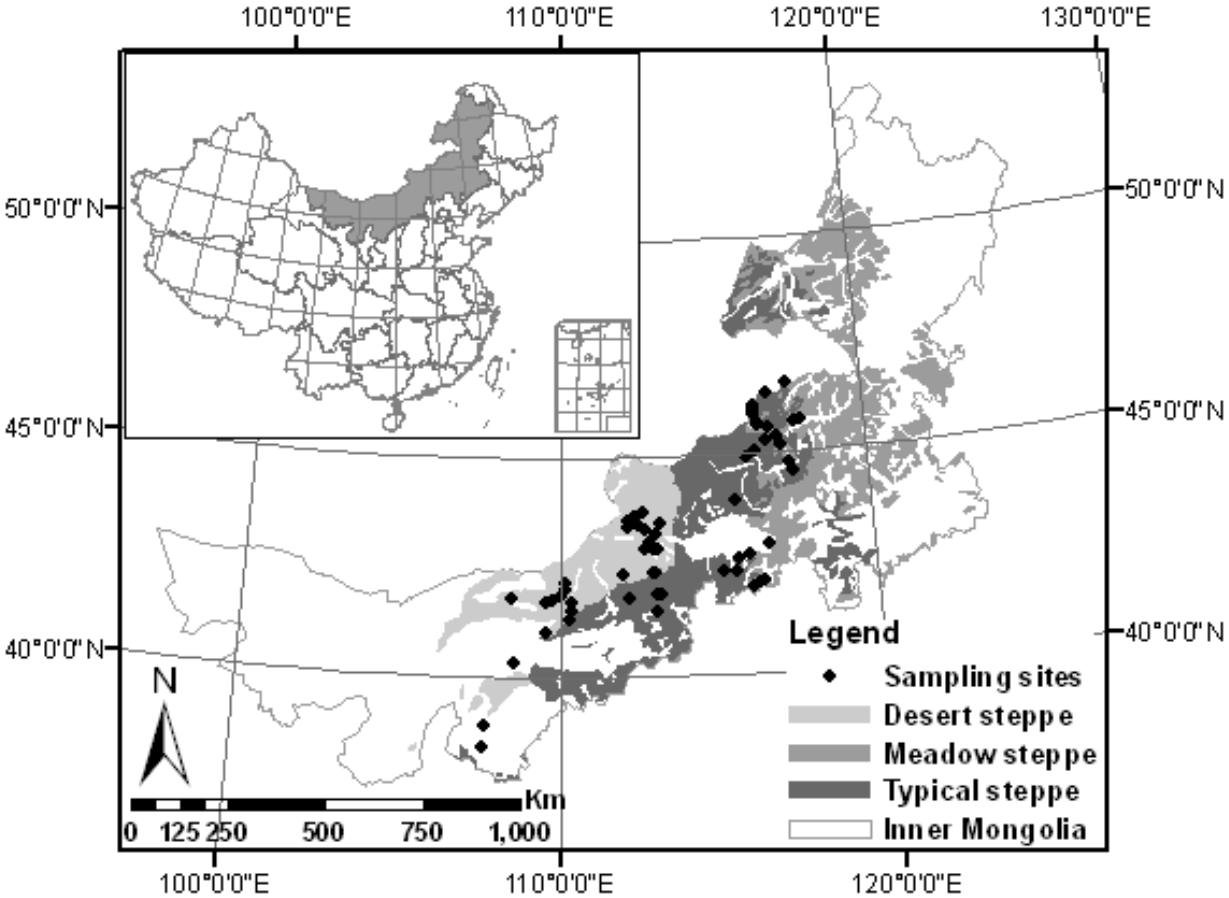

Figure 2. Changes in spectral reflectance of (a) 2006 and 2007, and (b) Class I, Class II, and Class III in Inner Mongolia

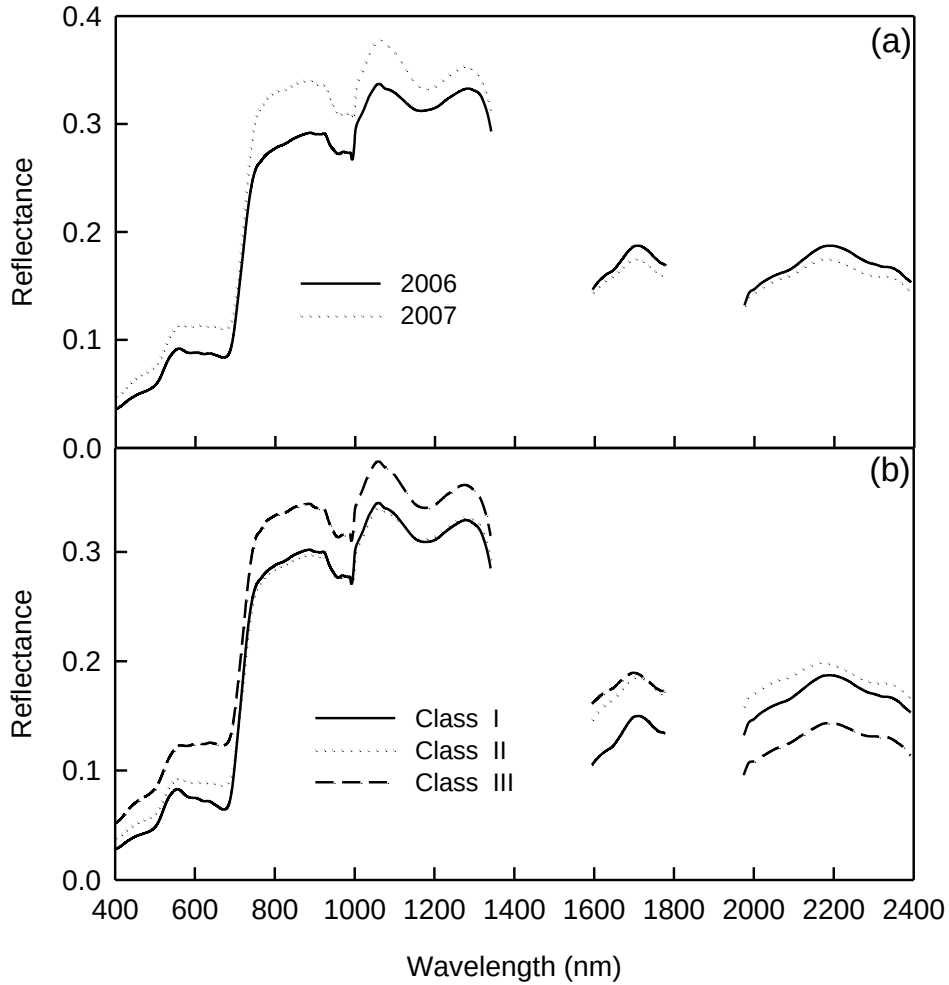

Table 1. Summary statistics of the biophysical characteristics from 61 sampled communities in Inner Mongolia.

	Min	Mean	Max	SD	Coefficient of variation
	The whole study area (n=61)				
PGC (%)	3.0	28.0	78.8	21.77	0.78
H (cm)	4.3	19.1	45.0	10.69	0.56
GBM (g m^{-2})	4.8	72.6	336.4	72.23	1.00
TBM (g m^{-2})	7.6	91.5	362.7	88.18	0.96
	Class I: less disturbances in typical steppe (n=11)				
PGC (%)	28.3	56.1	78.8	16.01	0.29
H (cm)	13.7	27.5	41.7	9.07	0.33
GBM (g m^{-2})	70.6	150.4	302.9	69.95	0.47
TBM (g m^{-2})	127.4	212.4	362.7	84.53	0.40
	Class II: more disturbances in typical steppe (n=24)				
PGC (%)	5.0	32.9	75.0	18.96	0.58
H (cm)	4.3	17.0	39.7	10.10	0.59
GBM (g m^{-2})	12.4	51.3	142.0	28.02	0.55
TBM (g m^{-2})	13.9	63.1	142.0	31.25	0.50
	Class III: desert steppe (n=26)				
PGC (%)	3.0	11.6	41.7	7.28	0.63
H (cm)	5.0	17.4	45.0	10.45	0.60
GBM (g m^{-2})	4.8	58.7	336.4	81.29	1.39
TBM (g m^{-2})	7.6	65.6	360.0	83.68	1.28

Table 2. Empirical models and performances from stepwise regressions using continuum-removed spectra and dr_{re} to estimate canopy properties (n=61).

	Spectra1	Spectra2	Spectra3	R^2
PGC	D_c	dr_{re}	D_{area}	0.41
H	D_c	-	-	0.30
GBM	D_c	dr_{re}	D_{area}	0.27
TBM	D_c	dr_{re}	D_{area}	0.31
$[\ln(PGC)]^{0.5}$	D_c	dr_{re}	D_{area}	0.54
$[\ln(H)]^{0.5}$	D_c	D_c/D_{area}	-	0.43
$[\ln(GBM)]^{0.5}$	D_c	dr_{re}	D_{area}	0.44
$[\ln(TBM)]^{0.5}$	D_c	dr_{re}	D_{area}	0.51

➔Old-growth Forests: carbon sink, or source:

Applications of eddy-covariance methods and interactions with meteorologists

Connections with other flux members: synthesis

Geographical distribution of the eddy flux tower sites involved in this analysis (Yi et al. Submitted)

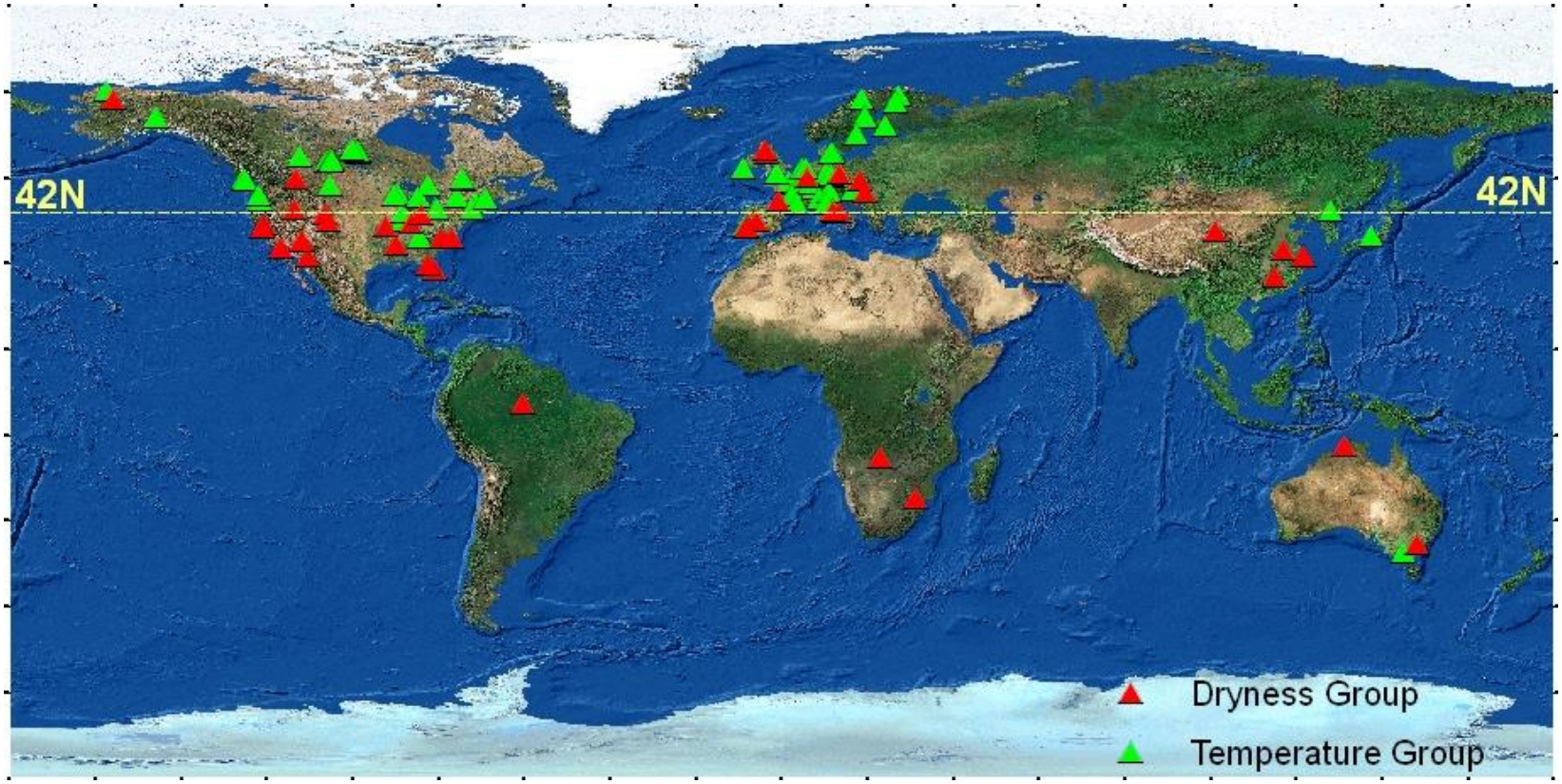

Cross-Lab Syntheses:

- Combined MODIS and AmeriFlux data for representative U.S. ecosystems to develop a predictive NEE model
- a gross carbon uptake between 6.91 and 7.33 Pg C yr^{-1} for the conterminous U.S. Drought, fires, and hurricanes reduced annual GPP at regional scales and could have a significant impact on the U.S. net ecosystem carbon exchange.
- The sources of the interannual variability of U.S. GPP were dominated by these extreme climate events and disturbances.

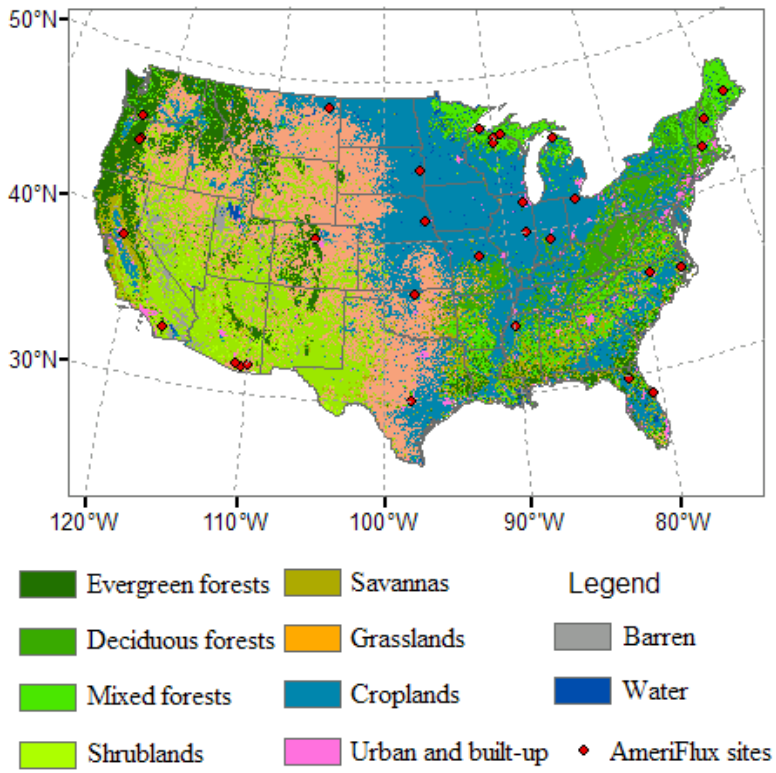

Xiao et al. (2008, 2010, 2011

JOURNAL OF GEOPHYSICAL RESEARCH, VOL. 117, G00J01, doi:10.1029/2011JG001889, 2012

Advances in upscaling of eddy covariance measurements of carbon and water fluxes

Jingfeng Xiao,[1] Jiquan Chen,[2] Kenneth J. Davis,[3] and Markus Reichstein[4]

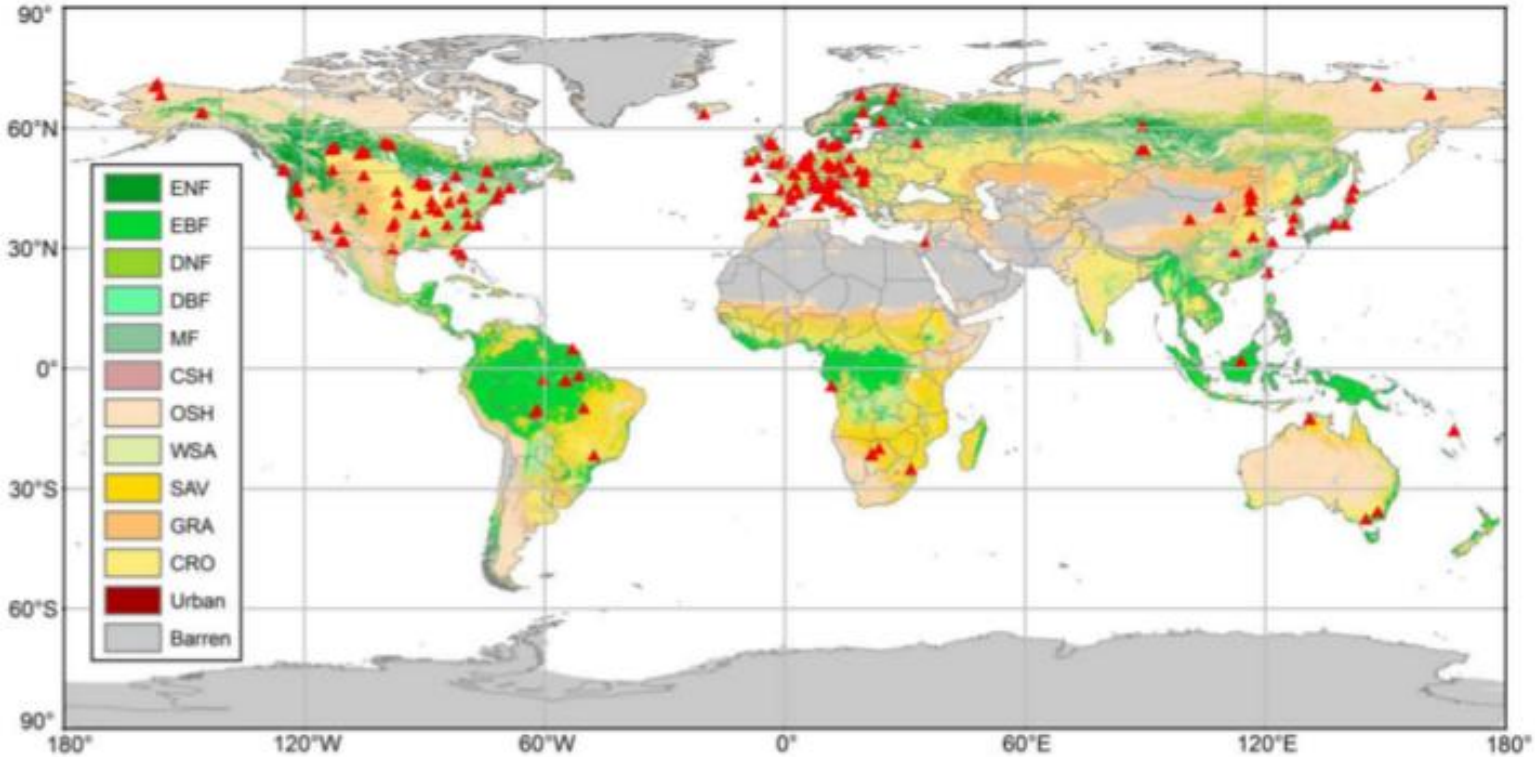

Figure 1. The location and distribution of eddy covariance flux towers involved in the FLUXNET synthesis database (also known as the LaThuile database). The symbols stand for flux towers. The base map is the Moderate Resolution Imaging Spectroradiometer (MODIS) land cover map, and the dominant land cover types include evergreen needle-leaf forests (ENF), evergreen broadleaf forests (EBF), deciduous needle-leaf forests (DNF), deciduous broadleaf forests (DBF), mixed forests (MF), closed shrublands (CSH), open shrublands (OSH), woody savannas (WSA), savannas (SAV), grasslands (GRA), croplands (CRO), urban and built-up (urban), and barren or sparsely vegetated (barren).

0, 2011

Climatic Change
DOI 10.1007/s10584-014-1234-9

Response of evapotranspiration and water availability to the changing climate in Northern Eurasia

Yaling Liu · Qianlai Zhuang · Zhihua Pan · Diego Miralles · Nadja Tchebakova · David Kicklighter · Jiquan Chen · Andrey Sirin · Yujie He · Guangsheng Zhou · Jerry Melillo

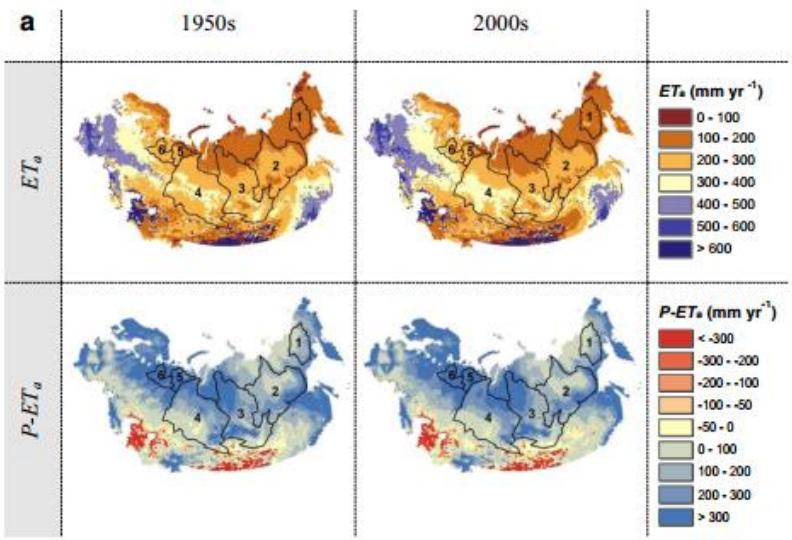

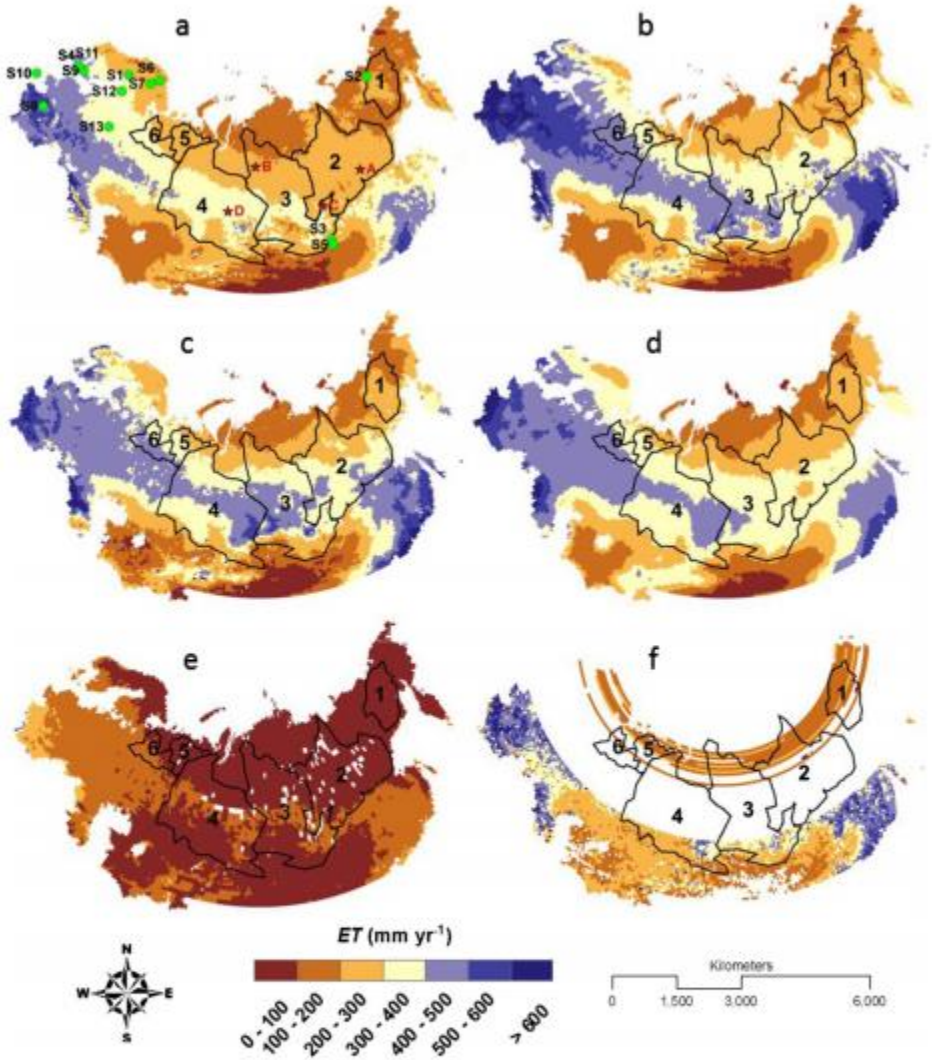

Fig. 1 Spatial patterns of average annual *ET* for uplands in the NE estimated by TEM and several satellite products: **a** TEM-AL1 *ET* during 2000–2009, **b** TEM-AL2 *ET* during 2000–2009, **c** GLEAM (Global Land-surface Evaporation: the Amsterdam Methodology) during 2000–2009, **d** the mean of LandFlux-EVAL merged synthesis product during 2000–2005, **e** PM-Mu *ET* during 2000–2007 in Vinukollu et al. (2011) and **f** MODIS-ET during 2000–2009. Areas with missing values or filled values are blanks on the map. The boundaries of six major river watersheds in the NE are delineated; 1, 2, 3, 4, 5 and 6 stand for Kolyma, Lena, Yenisei, Ob, Pechora and Northern Dvina watershed, respectively. The 13 EC sites and the four grid cells used for the simulation experiment are also shown on a), where EC site codes (S1–S13) and cell codes (A-D) correspond to those in Table S4 and Table S8 (Supplementary Materials), respectively. Note that the boundaries and numbers remain the same for all maps in this study

Remote Sensing of Environment 124 (2012) 717–729

Contents lists available at SciVerse ScienceDirect

Remote Sensing of Environment

journal homepage: www.elsevier.com/locate/rse

Evaluating spatial and temporal patterns of MODIS GPP over the conterminous U.S. against flux measurements and a process model

Fangmin Zhang [a,b,*], Jing M. Chen [b], Jiquan Chen [c], Christopher M. Gough [d], Timothy A. Martin [e], Danilo Dragoni [f]

[a] Jiangsu Key laboratory of Agricultural Meteorology, College of Applied Meteorology, Nanjing University of Information Science and Technology, Nanjing, 210044, China
[b] Department of Geography and Program in Planning, University of Toronto, Toronto, Canada M5S 3G3
[c] Department of Environmental Sciences, University of Toledo, Toledo, OH 43606-3390, USA
[d] Virginia Commonwealth University, Richmond, VA 23284-2012, USA
[e] School of Forest Resources and Conservation, University of Florida, Gainesville, FL 32611-0410, USA
[f] Department of Geography, Indiana University, Bloomington, IN 47405, USA

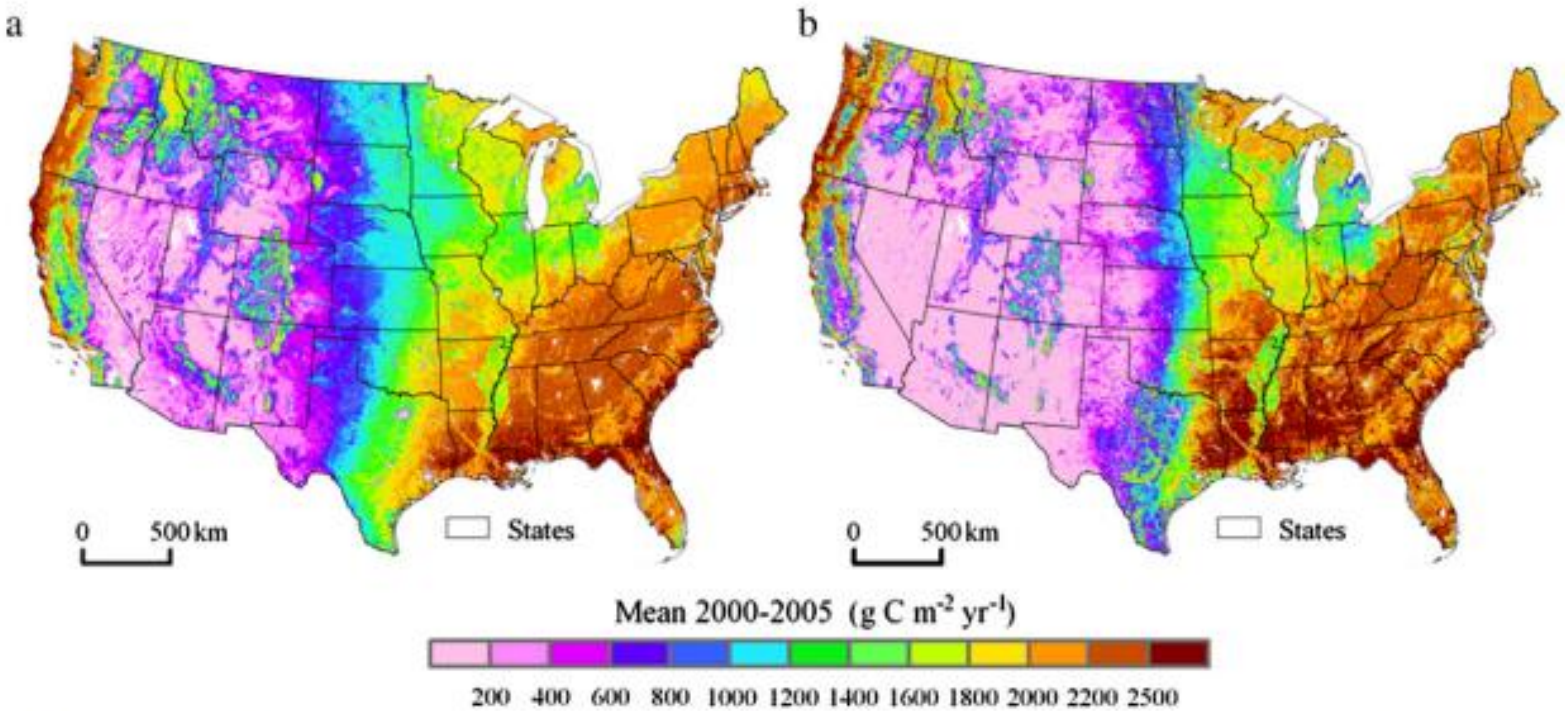

Fig. 4. The spatial distributions of annual gross primary productivity (GPP) over the conterminous U.S. by (a) the MODIS algorithm and (b) the BEPS model.

AGU PUBLICATIONS

JGR

Journal of Geophysical Research: Atmospheres

RESEARCH ARTICLE

10.1002/2013JD020864

Key Points:

- BMA-based latent heat flux estimation
- Global terrestrial LE estimation
- Integrating five process-based algorithms

Bayesian multimodel estimation of global terrestrial latent heat flux from eddy covariance, meteorological, and satellite observations

Yunjun Yao[1], Shunlin Liang[1,2], Xianglan Li[1], Yang Hong[3,4], Joshua B. Fisher[5], Nannan Zhang[6], Jiquan Chen[7], Jie Cheng[1], Shaohua Zhao[8], Xiaotong Zhang[1], Bo Jiang[1], Liang Sun[9], Kun Jia[1], Kaicun Wang[10], Yang Chen[10], Qiaozhen Mu[11], and Fei Feng[1]

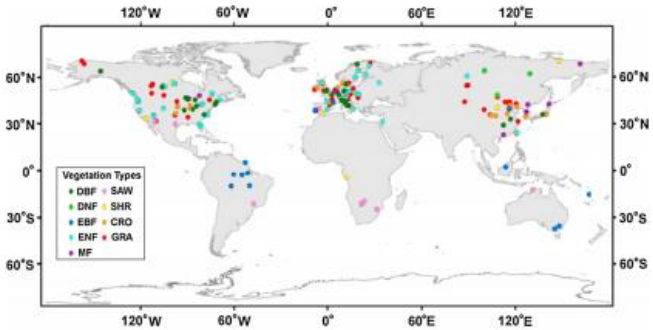

Figure 1. Locations of the 240 eddy covariance flux towers used in this study.

Table 2. Summary of the Five Process-Based LE Algorithms and Forcing Input Variables

LE Algorithm	Forcing Inputs	Institute	References
MODIS LE products algorithm (MOD16)	R_n, T_a, T_{min}, e, RH, LAI, land cover, FPAR	Numerical Terradynamic Simulation Group Department of Ecosystem and Conservation Sciences, University of Montana, USA	*Mu et al.* [2011]
Revised remote-sensing-based Penman-Monteith LE algorithm (RRS-PM)	R_n, T_a, e, RH, LAI, EVI	State Key Laboratory of Earth Surface Processes and Resource Ecology, Beijing Normal University, China	*Yuan et al.* [2010]
Priestley-Taylor LE algorithm of Jet Propulsion Laboratory, Caltech (PT-JPL)	R_n, T_a, T_{max}, e, RH, LAI, NDVI, FPAR	Jet Propulsion Laboratory, California Institute of Technology, USA	*Fisher et al.* [2008]
Modified satellite-based Priestley-Taylor LE algorithm (MS-PT)	R_n, T_a, T_{max}, T_{min}, NDVI	State Key Laboratory of Remote Sensing Science, Beijing Normal University, China	*Yao et al.* [2013]
Semiempirical Penman LE algorithm of the University of Maryland (UMD-SEMI)	R_s, T_a, e, WS, RH, NDVI	Department of Geography, University of Maryland, College Park, Maryland, USA	*Wang et al.* [2010a]

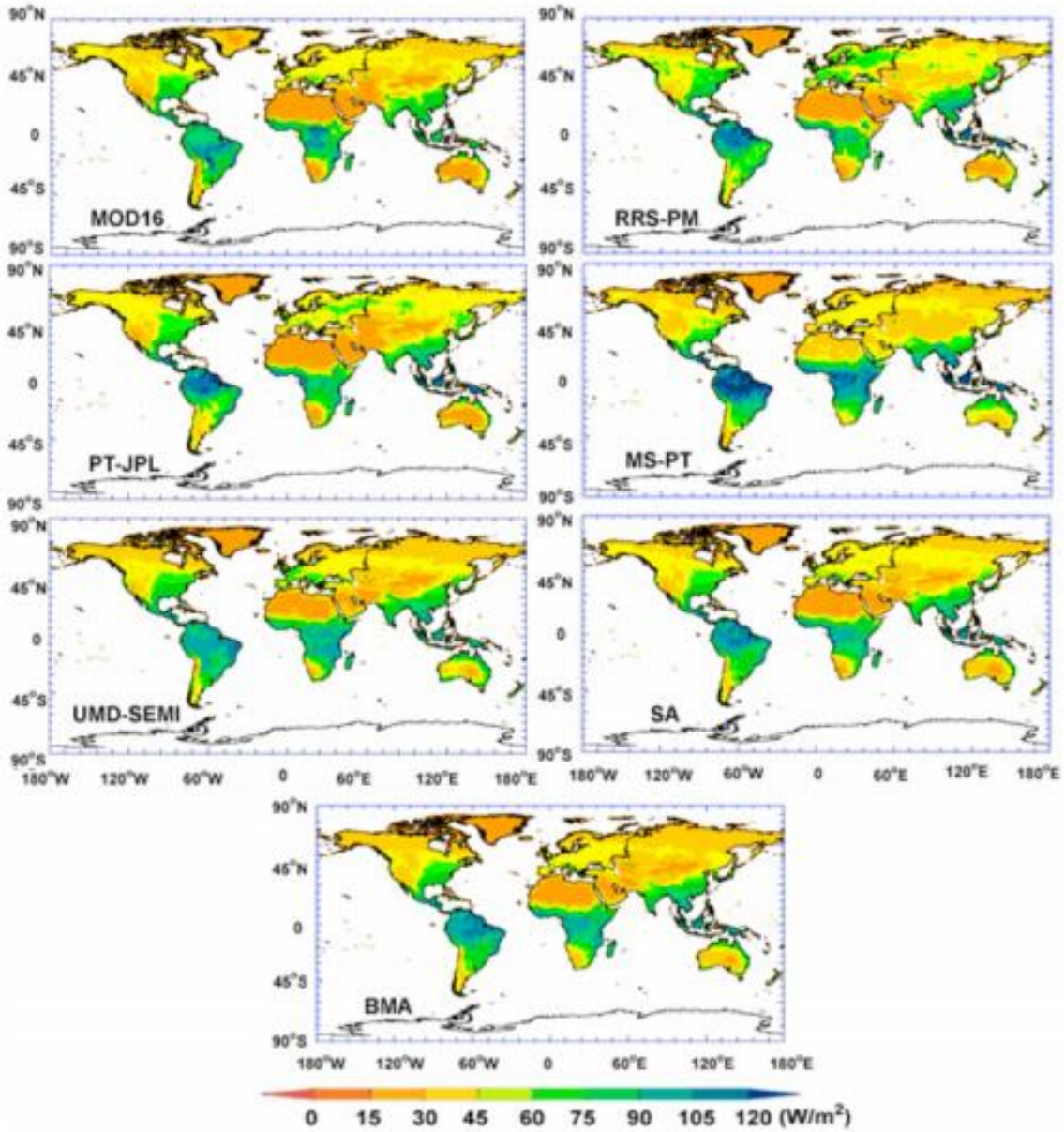

Figure 10. Maps of annual global terrestrial LE averaged for 2001–2004 at spatial resolution of 0.05° according to five process-based algorithms, the SA method, and the BMA method driven by GMAO-MERRA meteorology.